# Experimental investigation of flutter boundary with controlled vibration levels

Sodja, Jurij; Roizner, Federico; De Breuker, Roeland; Karpel, Moti

**Publication date**
2017

**Document Version**
Accepted author manuscript

**Published in**
17th International Forum on Aeroelasticity and Structural Dynamics, IFASD 2017

**Citation (APA)**
Sodja, J., Roizner, F., De Breuker, R., & Karpel, M. (2017). Experimental investigation of flutter boundary with controlled vibration levels. In *17th International Forum on Aeroelasticity and Structural Dynamics, IFASD 2017* (Vol. 2017-June). International Forum on Aeroelasticity and Structural Dynamics (IFASD).

# Experimental investigation of flutter boundary with controlled vibration levels

J. Sodja[a,*], F. Roizner[b], R. De Breuker[a], M. Karpel[b]

[a] *Faculty of Aerospace Engineering, Delft University of Technology, The Netherlands* [b]
*Faculty of Aerospace Engineering, Technion - Israel Institute of Technology, Israel*

**Abstract**

The first experimental application of the Parametric Flutter Margin method for identification of aeroelastic instabilities is presented. The experiment was performed in two steps using a two degree-of-freedom wing segment mounted in the wind tunnel. First, the reference flutter and divergence conditions were found by increasing the free-stream velocity until the observed response diverged. Then, the system was stabilized according to the Parametric Flutter Margin methodology, and the flutter and divergence conditions of the original test model were identified positively while being in a stable regime demonstrating excellent agreement with the reference instability conditions. Although the new experimental methodology is not model based, the results were compared with a theoretical model showing good agreement as well. The acquired data demonstrates both the accuracy of the Parametric Flutter Margin method as well as its capability to test for aeroelastic instabilities, both flutter and divergence, in stable and predictable testing conditions.

*Keywords:* Aeroelasticity, Parametric Flutter Margin, Flutter, Divergence, Characterisation, Wind tunnel Experiment

**Nomenclature**

| | | |
|---|---|---|
| $[A(i\omega)]$ | = | PFM system matrix |
| $\{B_f\}$ | = | Distribution vector, $\{B_f\} = [1, x_s]^T$ |
| $C(k)$ | = | Theodorsen function |
| $C_0$ | = | Airfoil centre of gravity |

*Corresponding author

*Email addresses:* j.sodja@tudelft.nl (J. Sodja), froizner@campus.technion.ac.il (F. Roizner), r.debreuker@tudelft.nl (R. De Breuker), karpel@technion.ac.il (M. Karpel)

$[C_f(i\omega)]$ = Acceleration sensor, $[C_f(i\omega)] = -\omega^2[1, x_s]$

$C_s$ = Location of the stabilising mass

$F_{ih}$ = Force measured by the impedance head

$F_s$ = External excitation force

$H(\omega; v_0)$ = Frequency response function

$J_0$ = Airfoil moment of inertia around $C_0$

$L$ = Lift

$M_0$ = Constant torque applied in divergence test

$M_{c/4}$ = Aerodynamic moment about point $Q$

$P$ = Airfoil hinge point

$Q$ = Quarter-chord point

$Y_f(\omega)$ = Gain function

$a$ = Non-dimensional location of $P$, $P = (1 + a)b$

$a_1, a_2$ = Acceleration measured by Accelerometer 1 and 2

$a_{ih}$ = Acceleration measured by the impedance head

$a_s$ = Acceleration of the stabilising mass

$b$ = Airfoil semi-chord, $b = c/2$

$c$ = Airfoil chord length

$d_h$ = Heave damping

$d_\theta$ = Pitch damping

$e_0$ = Non-dimensional location of $C_0$, $C_0 = (1 + e_0)b$

$e_s$ = Non-dimensional location of $C_s$, $C_s = (1 + e_s)b$

$h$ = Heave DOF

$h_{LVDT}$ = Heave DOF measured by the LVDT

$k$ = Reduced frequency, $k = \omega b/v_0$

$k_h$ = Heave stiffness

$k_s$ = Stiffness of the extensional spring

$k_\theta$ = Pitch stiffness

$k_\theta^s$ = Stabilising torsional stiffness

$m_*$ = Support mechanism mass

$m_0$ = Airfoil mass

$r$ = Dimensionless radius of gyration about $P$, $r^2 = (J_0 + m_0 x_0^2 b^2)/(m_0 b^2)$

$r_p$ = Pulley radius

$r_p^s$ = Pulley radius in divergence test for stabilisation stiffness

$r_{p1}$ = Pulley radius in divergence test with wind-on conditions

$t$ = Time

$u_f$ = Excitation input

$v_0$ = Freestream velocity

$v_d$ = Divergence speed

$v_f$ = Flutter speed

$x_0$ = Eccentricity of the airfoil section, $x_0 = e_0 - a$

$x_s$ = Eccentricity of the stabilising mass, $x_s = e_s - a$

$y_f$ = Acceleration in heave DOF at $C_s$

$\zeta(i\omega)$ = Vector of DOFs, $\zeta(i\omega) = [\xi, \theta]^T$

$\eta_\theta$ = Normalised damping coefficient of the pitch DOF, $\eta_\theta = d_\theta/(m_0 b^2)$

$\eta_\xi$ = Normalised damping coefficient of the heave DOF, $\eta_\xi = d_h/(m_0 b)$

$\theta$ = Non-dimensional pitch DOF

$\theta_{RVDT}$ = Pitch DOF measured by RVDT

$\theta_s$ = Pitch DOF deflection due to $M_0$

$\mu_*$ = Support to section mass ratio, $\mu_* = m^*/m_0$

$\mu_s$ = Stabilising to section mass ratio, $\mu_s = m_s/m_0$

$\xi$ = Non-dimensional heave DOF , $\xi = h/b$

$\rho$ = Air density

$\Phi_f(\omega)$ = Phase function

$\chi_\theta$ = Force in the pitch DOF

$\chi_\xi$ = Force in the heave DOF

| | | |
|---|---|---|
| $\omega_{pco}$ | = | Phase cross-over frequency |
| $\omega_\theta$ | = | Circular frequency of the pitch DOF, $\omega_\theta = \sqrt{k_\theta/J_0 + m_0 x_0^2 b^2}$ |
| $\omega_\xi$ | = | Circular frequency of the heave DOF, $\omega_\xi = \sqrt{k_h/m_0}$ |
| $\mathcal{AR}$ | = | Wing aspect ratio |
| ARMA | = | Autoregressive moving average |
| CG | = | Centre of gravity |
| DOF | = | Degree of freedom |
| FFT | = | Fast Fourier transform |
| FRF | = | Frequency response function |
| LVDT | = | Linear variable differential transformer |
| PFM | = | Parametric flutter margin |
| RVDT | = | Rotary variable differential transformer |
| SDOF | = | Single degree of freedom |

## 1. Introduction

Flight testing, used to prove that the aircraft flight envelope is flutter free, is a risky task. The flutter boundary is cautiously approached by gradually increasing the flight speed until the flight envelope is reached or a damping coefficient reaches the 3% threshold[1]. Meanwhile, the aircraft response to various sources of excitation like atmospheric turbulence or control surface deflections is continuously monitored and analysed. In some cases, such as explosive flutter, damping might suddenly rapidly decrease. Hence flutter might be encountered by accident causing severe damage to the aircraft. Consequently, such tests are accompanied by numerous numerical analyses, wind tunnel and ground testing to avoid bringing the tested aircraft too close to the flutter boundary by accident[1].

Various flight-test data-analysis methods are available for application in on- and off-line manner to identify the flutter conditions. Among others: damping extrapolation[2], envelope function[3], the Zimmerman-Weissenburger flutter margin[4], the model-based flutterometer method[5], and using a discrete-time autoregressive moving average (ARMA) model[6]. Operating at flutter conditions might have catastrophic results. Therefore, all the approaches rely, in one way or another, on extrapolation to predict the flutter conditions while staying at safe flying conditions, which makes the tests expensive, time-consuming and risky. On the contrary, the recently developed Parametric Flutter Margin (PFM) method[7] is based on analysing frequency-response functions (FRFs) at and beyond the nominal flutter onset conditions, but with the system modified such that it is actually stable. This allows us to identify flutter positively without exceeding the pre-determined safe vibration levels. It is anticipated that the PFM methodology will be very instrumental in the design of future flutter-test campaigns improving their safety and reduce the time and effort required to ensure that the flight envelope is indeed flutter free.

Karpel and Roizner[8] proposed a novel method for finding the flutter boundary experimentally based on their numerical PFM method[7]. The experimental PFM mitigates some of the deficiencies of the currently established methods, namely the need to approach the flutter boundary cautiously, and the fact that the flutter boundary is never positively identified unless erroneously encountered. The PFM method is based on the idea that the stability point of an aeroelastic system can be offset by adding a stabilising element. In the case of wing flutter, such a stabilising element could be an added mass at the leading edge of the wing tip. Such an augmented system is then subjected to harmonic excitation to obtain the FRF of the stabilising element, for instance, the acceleration of the added mass which is then analysed for gain margin at phase-cross-over (pco) frequency. The flutter boundary of the original system excluding the added stabilising mass is reached when the gain margin of the stabilising element equals 0dB. The FRF analysis is repeated at various flight conditions to obtain the gain margin vs flight speed characteristics. The flutter speed is read from the graph at 0dB. Details on the theoretical foundation of the PFM method and its formulation are provided in Roizner and Karpel[7] while

the key equations and their application related to this experiment are outlined in this paper.

It is worth pointing out that the PFM method allows for the flutter boundary identification of the original system excluding the added mass while the augmented system remains stable. This greatly reduces the risk of such experimental efforts.

The contribution to the state of the art of this paper is a proof of concept and validation of the proposed PFM method using a typical wing section with pitch and plunge degrees of freedom (DOF) mounted in the wind tunnel. The paper is organized as follows: in Sec. 2 the mathematical formulation of the 2DOF aeroelastic system along with its PFM implementation related to the experiment is presented, Sec. 3 describes the experimental setup and the testing procedure. The results are shown in Sec. 4, and the conclusions of this work are given in Sec. 5.

## 2. Theoretical Model of the Aeroelastic System

The mathematical formulation of the 2DOF airfoil along with its PFM implementation relevant to this experiment is presented in this section. The mathematical model had three main purposes. First, to configure the experimental setup to obtain the aeroelastic instability at a velocity within the wind tunnel capabilities. Second, to size and position the stabilizing weight such that the flutter velocity would increase by at least 15%, and the third purpose was the comparison with the experimental results. It has to be stressed, however, that the experimental PFM method or its results do not depend on the application of this mathematical model. The experimental PFM method is not model-based and does not require any mathematical model of the aeroelastic system to identify the nominal flutter conditions if they exist in the test velocity range.

First, the governing equations of motion are presented, followed by the presentation of the PFM methodology.

### *2.1. Equation of Motion*

The experimental aeroelastic system was modelled using a typical section with pitch and heave DOFs as depicted in Fig. 1. The airfoil of chord length $2b$, mass $m_0$ and moment of inertia $J_0$ expressed around the centre of gravity at $C_0$ is hinged at the point $P$. Additionally, $m_*$ represents all the additional support mass, such as the mass of the pitching mechanism, supported by the leaf springs governing the heaving motion. This mass is involved in the heave motion only and does not contribute to the overall moment of inertia involved in the pitching motion. Stiffness and damping characteristics of the pitch and heave DOFs are presented by $k_\theta$ and $d_\theta$, and $k_h$ and $d_h$, respectively. Lift $L$, and aerodynamic moment $M_{c/4}$ are assumed to act at the quarter-chord point $Q$. The external excitation force $F_s$ is applied at the same location as the stabilising mass, at point $C_s$. The points $P$, $C_0$ and $C_s$ are expressed in terms of the airfoil half chord $b$ and non-dimensional parameters $a$, $e_0$ and $e_s$ which can assume

values between [-1, 1], with -1 being the airfoil leading edge and 1 the airfoil trailing edge. The response of the wing section to $L$, $F_s$, and $M_{c/4}$ is governed by the following equation of motion:

$$\begin{bmatrix} 1+\mu_* & x_0 \\ x_0 & r^2 \end{bmatrix} \begin{Bmatrix} \ddot{\xi} \\ \ddot{\theta} \end{Bmatrix} + \begin{bmatrix} \eta_\xi & 0 \\ 0 & \eta_\theta \end{bmatrix} \begin{Bmatrix} \dot{\xi} \\ \dot{\theta} \end{Bmatrix} + \begin{bmatrix} \omega_\xi^2 & 0 \\ 0 & r^2\omega_\theta^2 \end{bmatrix} \begin{Bmatrix} \xi \\ \theta \end{Bmatrix} = \begin{Bmatrix} \chi_\xi \\ \chi_\theta \end{Bmatrix} \tag{1}$$

where $\xi = h/b$ and $\theta$ represent dimensionless heave and pitch DOFs. $x_0 = e_0 - a$ is the eccentricity parameter of the airfoil section. $r^2 = (J_0 + m_0 x_0^2 b^2)/(m_0 b^2)$ represents the dimensionless radius of gyration of the wing section about the pivot point $P$. $\mu_* = m_*/m_0$ is the ratio between the support mass and the section mass. $\eta_\xi = d_h/(m_0 b)$ and $\eta_\theta = d_\theta/(m_0 b^2)$, $\omega_\xi = \sqrt{k_h/m_0}$ and $\omega_\theta = \sqrt{k_\theta/(J_0 + m_0 x_\theta^2 b^2)}$ are the normalised damping coefficients and the circular frequencies of the heave and pitch DOF, respectively. Finally, $\chi_\xi$ and $\chi_\theta$ are the forces of the corresponding DOFs given as:

$$\begin{aligned} \chi_\xi &= \frac{1}{m_0 b}\left(-L + F_s\right) \\ \chi_\theta &= \frac{1}{m_0 b^2}\left(M_{c/4} + (1/2 + a)\, bL + x_s b F_s\right) \end{aligned} \tag{2}$$

where $x_s = e_s - a$ is the eccentricity parameter of the stabilising mass. The relative thickness of the sections airfoil is 12%, the excitation force $F_s = \hat{F}_s e^{i\omega t}$ is harmonic, hence unsteady thin-airfoil theory and harmonic motion of the section are valid assumptions. Consequently, $L$ and $M_{c/4}$ can be expressed using the Theodorsen theory [9] as:

$$\begin{aligned} L &= 2\pi\rho v_\infty b^2 C(k)\left(\dot{\xi} + \frac{v_0}{b}\theta + \left(\frac{1}{2} - a\right)\dot{\theta}\right) + \pi\rho b^3\left(\ddot{\xi} + \frac{v_0}{b}\dot{\theta} - a\ddot{\theta}\right) \\ M_{c/4} &= -\pi\rho b^4\left(\frac{1}{2}\ddot{\xi} + \frac{v_0}{b}\dot{\theta} + \left(\frac{1}{8} - \frac{a}{2}\right)\ddot{\theta}\right) \end{aligned} \tag{3}$$

where $C(k)$ represents the Theodorsen function, $k$ the reduced frequency, $v_0$ the airstream velocity and $\rho$ the air density.

### *2.2. Parametric Flutter Margin Method*

The implementation of the PFM method [7] for identifying flutter of the 2DOF airfoil using a stabilizing mass is outlined in this subsection. The flutter equation is obtained by transforming Eq. 1 to frequency domain (FD) and setting the external excitation to zero. Accordingly, Eq. 1 becomes:

$$\left[A(i\omega)\right]\left\{\zeta(i\omega)\right\} = \left\{0\right\} \tag{4}$$

where $\zeta(i\omega) = [\xi, \theta]^T$. The system matrix $[A(i\omega)]$ contains the structural mass, damping and stiffness matrices, and the frequency-depended aerodynamic coefficient matrix. Flutter conditions are defined mathematically as the flight

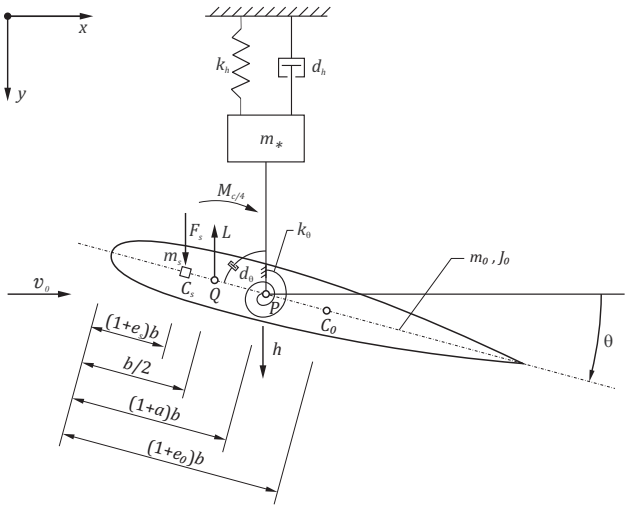


Figure 1: Typical section with pitch and heave DOF

parameters at which Eq. 4 yields a non-trivial solution. Accordingly, common flutter methods such as the p-k[10] and k-methods[11] search for flutter by zeroing the system matrix determinant $|A(i\omega)| = 0$.

The PFM procedure, on the other hand, searches for the flutter boundary using FRFs obtained by the excitation introduced in the right side of Eq. 4. However, the response of the original system approaches infinity at the stability boundary. Hence, FRFs are calculated with $[A(i\omega)]$ modified to include the effect of a stabilizing parameter and to avoid the numerical issues of dealing with the infinite response of the original system. In our case, a mass represented by $\mu_s = m_s/m_0$ located at $C_s$ is used as a stabilizing element. The flutter conditions are found by measuring the acceleration at $C_s$, represented by $y_f$. The equation of motion with the added stabilizing element is:

$$\begin{aligned} \left[A(i\omega) + \mu_s \left\{B_f\right\} \left[C_f(i\omega)\right]\right] \left\{\zeta(i\omega)\right\} &= \left\{B_f\right\} u_f(i\omega) \\ y(i\omega) &= \left[C_f(i\omega)\right] \left\{\zeta(i\omega)\right\} \end{aligned} \tag{5}$$

where $u_f$ is the excitation input, which represents the amplitude of the excitation applied at $C_s$, distributed to the system through $\{B_f\} = [1, x_s]^T$, and $[C_f(i\omega)] = -\omega^2[1, x_s]$ defines the acceleration sensor. For a given $u_f(i\omega)$ one can solve Eq. 5 for $\{\zeta(i\omega)\}$ and $y_f(i\omega)$ at all stable flight points of the stabilised aeroelastic system, including at the nominal flutter point of the original system which is now stable. Furthermore, the flight conditions and the excitation frequency for which the complex equation

$$u_f(i\omega_f) = \mu_s y_f(i\omega_f) \tag{6}$$

is satisfied must reflect the flutter-onset conditions because the added terms vanish and Eq. 5 reduces back to the homogeneous Eq. 4. The calculated

$\{\zeta(i\omega_f)\}$ is the non-trivial solution of Eq. 4, namely the flutter mode. At other velocity points, where $y_f(i\omega)$ and $u_f(i\omega)$ are of the same phase, but Eq. 6 is not satisfied, the ratio $\mu_s y_f(i\omega)/u_f(i\omega)$ defines the flutter margin with respect to $\mu_s$.

The PFM flutter analysis starts with calculating $y_f(i\omega)$ in response to $u_f(i\omega)$. To find the flutter onset conditions, in which Eq. 6 is satisfied in both magnitude and phase, response functions are first generated at various velocities at constant altitude. Bode plots are then generated in terms of real-valued gain and phase functions:

$$\begin{aligned} Y_f(\omega) &= 20\log|\mu_s y_f(i\omega)/u_f(i\omega)| \\ \Phi_f(\omega) &= \angle\left(\mu_s y_f(i\omega)/u_f(i\omega)\right) \end{aligned} \tag{7}$$

These plots are then used for calculating the phase cross-over gains $Y_f(\omega_{pco})$, where $\omega_{pco}$ is a phase-cross-over frequency at which $\Phi_f(\omega_{pco}) = 360\text{deg}$. The original system would be neutrally stable at the interpolated velocity $v_f$ where $Y_f(\omega_{pco}) = 0\text{dB}$. The corresponding flutter frequency and the complex flutter mode of the original system equal to: $\omega_f = \omega_{pco}$ and $\{\zeta_f(i\omega_{pco})\}$, respectively.

## 3. Experiment

### *3.1. Experimental Setup*

The experimental setup developed by Gjerek et al.[12] was used in this work as it has a well-defined pitch and heave DOFs with the possibility to adjust the stiffness of each DOF individually. In addition, other important parameters governing the aeroelastic response of the airfoil, such as pitch axis, centre of gravity location, mass and moment of inertia, can be varied. As a result, various aeroelastic configurations can be easily studied, and the apparatus can be tailored to meet the requirements of the wind tunnel and those of the PFM method. The apparatus is shown in Fig. 2.

The heave mechanism consists of two pairs of cantilever leaf springs at the top and bottom of the apparatus as shown in Fig. 2. The heave stiffness, $k_h$, can be adjusted by changing the length of the leaf springs. The heave mechanism also supports the pitch mechanism, which governs the torsional stiffness and provides support to the rigid airfoil. The pitch mechanism is shown in more detail in Fig. 3a. Torsional stiffness is introduced by a pair of preloaded extension springs attached to the pulley which is mounted on the axle of the rigid airfoil. Torsional stiffness can be adjusted by changing the extensional springs or the diameter of the pulley. Both mechanisms are placed outside the test section not to obstruct the airflow.

The stabilising weight is mounted by a pair of aluminium rods attached to the axle of the airfoil outside the test section as shown in Fig. 3b. The mass of the stabilising weight as well as its distance from the rotational axis can be adjusted to achieve sufficient increase of the flutter speed for safe application of the PFM method.

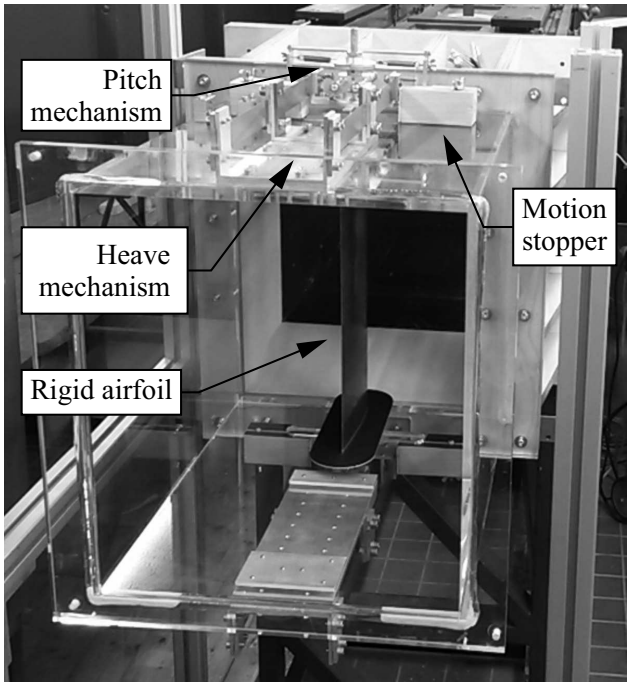


Figure 2: Experimental setup

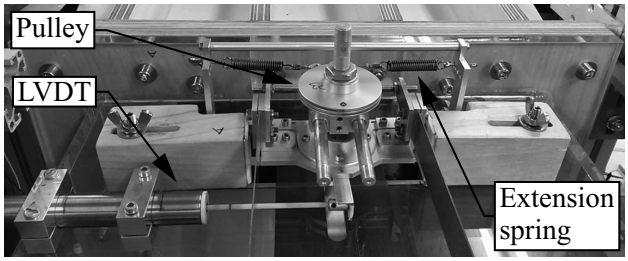


(a) Pitch mechanism

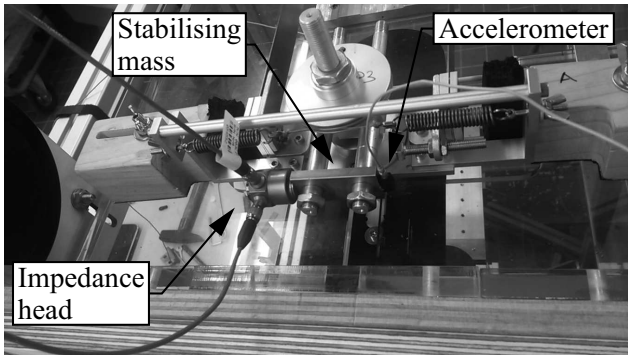


(b) Stabilising mass with impedance head and accelerometer

Figure 3: Details of the experimental setup

Table 1: Physical properties of the experimental setup

| Parameter | Unit | Quantity |
|---|---|---|
| airfoil | [−] | NACA 0012 |
| chord×span, $2b \times s$ | [m$^2$] | 0.16×0.36 |
| airfoil mass, $m_0$ | [kg] | 0.622 |
| heave mass, $m^*$ | [kg] | 0.441 |
| moment of inertia, $J_0$ | [kgm$^2$] | $1.92 \cdot 10^{-3}$ |
| axis of rotation, $(1+a)b$ | [m] | 0.064 |
| CG, $(1+e_0)b$ | [m] | 0.067 |
| heave stiffness, $k_h$ | [N/m] | 710 |
| heave damping, $D_h$ | [Ns/m] | 1.5 |
| pitch stiffness, $k_\theta$ | [Nm/rad] | 1.65, 3.14$^\dagger$ |
| pitch damping, $D_\theta$ | [Nms/rad] | 0.0066, 0.0035$^\dagger$ |

$^\dagger$ Values pertinent to Configurations 1 and 2, respectively.

Both pitch and heave DOF were limited with physical motion stoppers which allowed direct measurement of the flutter onset conditions by increasing the air velocity in the wind tunnel until flutter was observed.

Based on the preliminary investigation two configurations were selected which physical properties are summarised in Table 1. The listed physical properties are already updated to agree with the results from the system identification tests. The main difference between the two selected configurations is the torsional stiffness $k_\theta$, which significantly alters the flutter and divergence boundary of the experimental setup. Torsional stiffness was set to 1.65Nm/rad and 3.14Nm/rad for Configuration 1 and Configuration 2, respectively.

### *3.2. Instrumentation and Excitation*

The aeroelastic response of the airfoil was monitored using displacement and rotation sensors, an impedance head and a set of accelerometers. The airfoil motion was measured using a linear and rotational variable differential transformer, LVDT and RVDT, attached to the axle of the airfoil. Placement of the sensors, their type and orientation are indicated in Fig. 4.

The PFM method requires to apply the force and to measure the resulting acceleration of the system at the stabilising weight location. Accordingly, an impedance head was used and mounted directly on the stabilising weight as depicted in Fig. 3b. Therewith, the gain, $Y_f$, and phase, $\Phi_f$, as defined by Eq. 7 can be measured directly. Redundant accelerometers, $a_1$ and $a_2$, were mounted on the axle of the airfoil and on the other side of the stabilising weight to provide control measurements.

Mass of the installed sensors has to be adequately accounted for. While the mass of the sensors attached directly to the airfoil is negligible relative to the airfoils mass, the mass of the sensors attached to the stabilising weight is not.

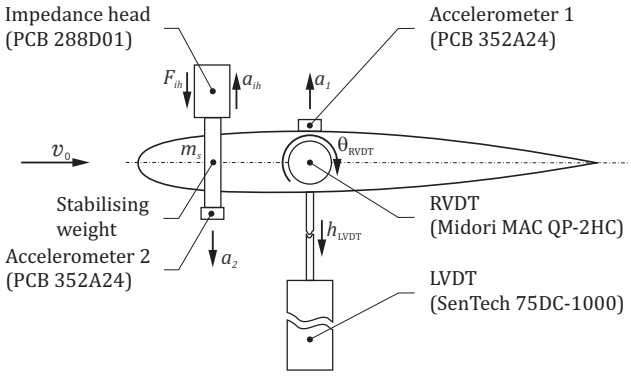


Figure 4: Instrumentation of the aeroelastic system

The impedance head and the control accelerometer with their pertinent cabling contribute 40% to the overall stabilising mass. These masses were hence added to the total stabilising mass used in the determination of the FRFs.

The excitation signal, $u_f(t)$, measured by the impedance head was an impulsive force provided by a hit of a hammer.

### *3.3. Testing Procedure*

Both of the selected configurations were tested for flutter while Configuration 1 was also tested for divergence. Two tests were performed for each case: using the conventional approach and the PFM method. This way, the aeroelastic stability boundary obtained using the PFM method could be directly compared to the flutter or divergence onset conditions observed on the original, non-augmented aeroelastic system.

#### *3.3.1. Flutter Test*

Flutter properties of each configuration were investigated first by monitoring the response of the original aeroelastic system to small perturbations while slowly increasing the airstream velocity in the wind tunnel. The system was excited manually by exerting a force impulse on the model such that both heave and plunge DOF were excited simultaneously to overcome the initial friction. The airstream velocity was increased until the flutter instability appeared.

In the next step, the aeroelastic system was augmented by adding the stabilising mass. Again, the same procedure was applied to establish the flutter properties of the augmented system and demonstrate that the augmented system remains stable at the flutter conditions of the original system.

For applying the PFM methodology, FRFs at selected airstream velocities, $v_0$, were determined by recording the time signal of the excitation force and the stabilising weights acceleration. The measured signals were converted to the frequency domain using the Fast Fourier transform (FFT), and the FRF was

calculated as:

$$H(\omega; v_0) = \frac{m_s a_s(\omega; v_0)}{F_s(\omega; v_0)} \tag{8}$$

where $a_s$ is the acceleration of the stabilising weight measured either by the impedance head or the accelerometer $a_2$ as depicted in Fig. 4. $m_s$ and $F_s$ are the mass of the stabilising weight and the external force as shown in Fig. 3. $F_s$ was applied directly to the stabilising weight and measured by the impedance head.

After obtaining sufficient FRFs over a range of $v_0$ the methodology outlined in Sec. 2.2 is used. The Bode plots are generated, and the experimental phase-cross-over frequencies and corresponding gains for each $v_0$ are determined. These, in turn, can be plotted as a function of $v_0$ which allows determining the flutter velocity and frequency, which equal to the airstream velocity and phase-cross-over frequency at which the phase-cross-over gain equals 0dB.

The excitation force can be applied in various ways, for example by using an electromechanical shaker or an impedance hammer, as long as it contains sufficient energy to excite the aeroelastic modes involved in the flutter mechanism. In the current experiment, a regular hammer was used for excitation since it did not constrain the motion of the aeroelastic system after applying the force.

*3.3.2. Divergence Test*

Similar to the flutter investigation, divergence was first determined in a conventional way followed by the application of the PFM method.

Configuration 1 of the aeroelastic system was used. In addition, enough stabilising mass was added to the aeroelastic system such that the divergence would become critical and would occur before flutter. Again, the airstream velocity was gradually increased, and the system response in terms of pitch and heave displacement to a small perturbation was measured. An example of such a measurement is shown below in Fig. 12a. The airstream velocity was increased until a sharp increase in the measured displacements was observed.

The PFM method is performed as follows in the case of divergence test. First, the aeroelastic system is stabilised by adding a stabilising torsional spring of stiffness $k_\theta^s$ to the pitch DOF in order to offset the divergence onset to a higher $v_0$. Then a constant torque, $M_0$, is applied to the pitch DOF and $\theta$ is measured while $v_0$ is increased. The original aeroelastic system diverges at $v_d$ when the torsional deflection of the augmented aeroelastic system satisfies the following condition:

$$\theta(v_d) = \theta^s = \left.\frac{M_0}{k_\theta^s}\right|_{v_0=0\text{m/s}} \tag{9}$$

where $\theta^s$ represents the torsional deflection of the pitch DOF under the applied torque $M_0$ at wind-off conditions, $v_0 = 0$m/s, if the torsional stiffness of the aeroelastic system would equal to the torsional stiffness of the stabilising spring only.

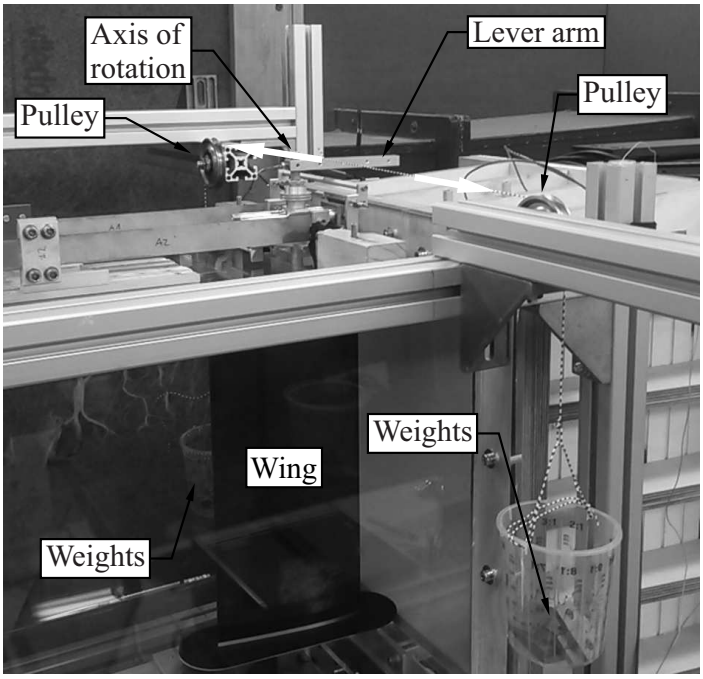


(a) Overview

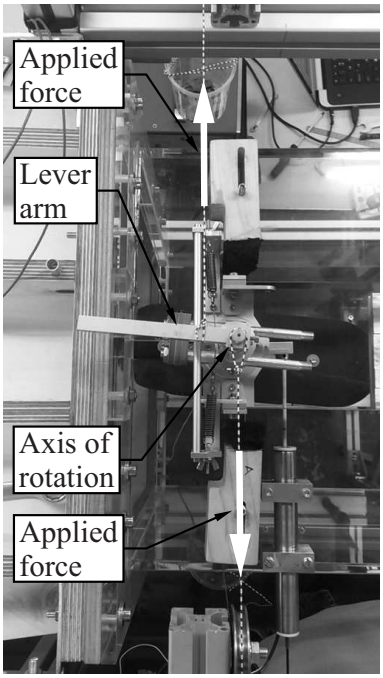


(b) Top view

Figure 5: Divergence setup

The torsional stiffness, $k_\theta$, of the aeroelastic system is governed by the pulley-spring mechanism, shown in Fig. 3a, as:

$$k_\theta = 2k_s r_p^2 \tag{10}$$

where $k_s$ represents the stiffness of the extensional springs and $r_p$ represents the pulley radius. Since a pulley can be easily exchanged, it was decided to introduce the stabilising torsional stiffness $k_\theta^s$ by swapping the pulley in the original aeroelastic system with a second pulley of a larger radius, $r_{p1}$, such that:

$$k_{\theta 1} = k_\theta + k_\theta^s \tag{11}$$

To be able to measure $\theta^s$, a third pulley of radius $r_p^s$ was machined such that

$$k_\theta^s = 2k_s(r_p^s)^2 \tag{12}$$

As a result, the actual PFM divergence test was performed in the following order. First, the pulley of radius $r_p^s$ was installed and $\theta^s$ at $M_0$ and $v_0 = 0$m/s was measured. Then the pulley of radius $r_{p1}$ was installed and $v_0$ was increased until the condition expressed by Eq. 9 was met.

The torque $M_0$ was applied by a force couple exerted by weights hanging from the pulley as shown in Fig. 5a. A top view of the lever arm and the cable attachment is shown in Fig. 5b.

## 4. Results and Discussion

Experimental results obtained during the wind tunnel campaign are presented and discussed in this section. System identification results are presented first, followed by the conventional and the PFM flutter tests. The divergence results are discussed at the end.

### *4.1. System Identification*

A system identification test was performed as part of the flutter tests when the aeroelastic system was fully assembled and mounted in the wind tunnel. This way stiffness and damping properties could be determined in order to update the theoretical model presented in Sec. 2.

System identification was performed by fitting a transfer function expressed by Eq. 7 to the measured response. Results for both Configuration 1 and 2 are shown in Fig. 6. The identified properties are included in Table 1. In general, good agreement between the measurements and the fitted response can be observed, especially in the range of frequencies that are of interest from the flutter investigation point of view, around 4.5Hz for Configuration 1 and 5.1Hz for Configuration 2.

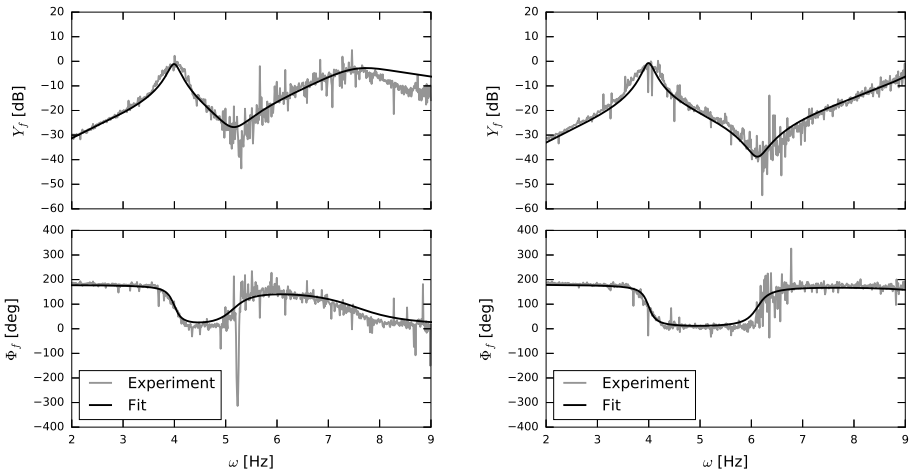


(a) Configuration 1

(b) Configuration 2

Figure 6: System identification

### *4.2. Flutter*

Flutter conditions were first identified for the original, non-augmented system following the procedure outlined in Sec. 3.3.1. Heave and pitch response to a small perturbation at two consecutive airstream velocities for the two investigated configurations are shown in Fig. 7. In the case of Configuration 1, a converging response is observed at $v_0 = 15.2$m/s and a diverging response at $v_0 = 15.4$m/s. Hence it was concluded that the flutter onset velocity of Configuration 1 is 15.3m/s.

In the case of Configuration 2, a converging response is observed at $v_0 = 22.5$m/s and a constant amplitude response at $v_0 = 22.7$m/s, which indicates that the damping is virtually zero and that the system is at the flutter boundary. Hence it was concluded that the flutter onset velocity pertinent to Configuration 2 is at 22.7m/s.

Measurement of the FRFs of the Eq. 5 and the extraction of the associated Bode plots defined by Eq. 7 lay at the heart of the PFM method. The Bode plots of the measured FRFs at three different airstream velocities and for each configuration are shown in Figs. 8a and 9a respectively. The experimental results are shown as grey lines. Despite the fact that these results were obtained by averaging over the response measured by both the impedance head and the control accelerometer, $a_2$, and over several excitation responses, one can still observe some noise present in the signal which renders the determination of the $\omega_{pco}$, and the corresponding gain, $Y_f(\omega_{pco})$, more difficult. Therefore, it was decided to fit a transfer function to the measurements as depicted by the full lines in Figs. 8a and 9a over a selected range of frequencies around the $\omega_{pco}$. Nevertheless, it is clear from the experimental result that once $v_0$ exceeds the flutter speed of the original system, $Y_f(\omega_{pco})$ exceeds 0dB.

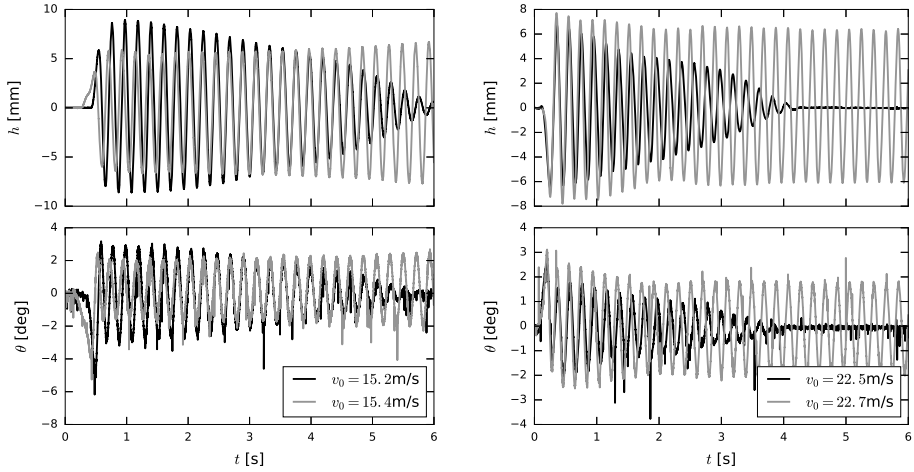


(a) Configuration 1 (b) Configuration 2

Figure 7: Flutter response

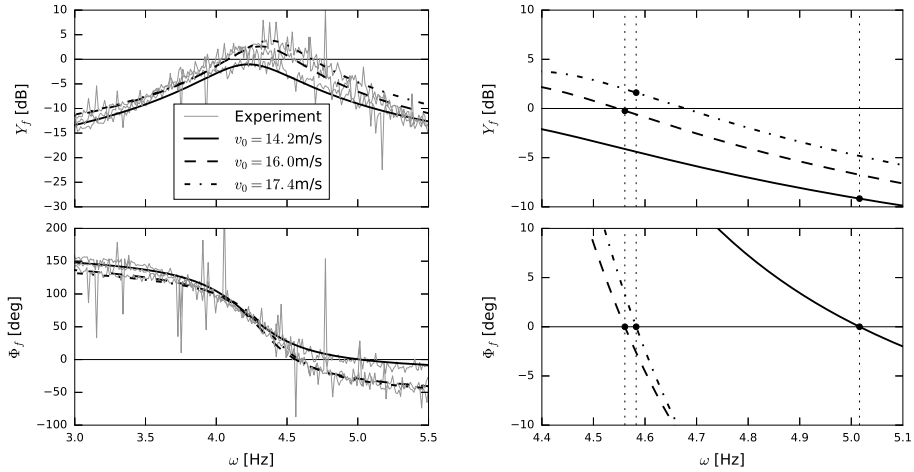


(a) Bode plot (b) Zoom-in

Figure 8: Frequency response: Configuration 1

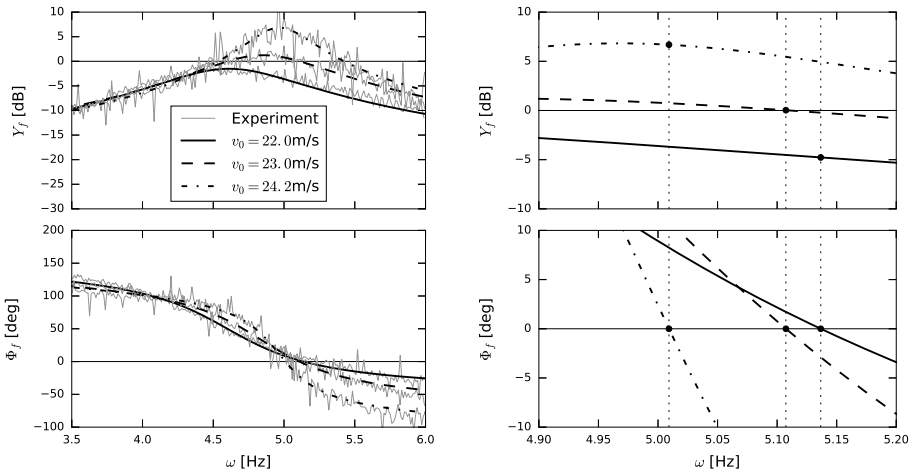


(a) Bode plot

(b) Zoom-in

Figure 9: Frequency response: Configuration 2

A transfer function used for fitting was in the form of a transfer function pertinent to a single degree of freedom (SDOF) harmonic oscillator with two complex-conjugate poles. Therewith smooth continuous Bode plots were obtained for the determination of $\omega_{pco}$ and the associated $Y_f(\omega_{pco})$. It is important to understand that the transfer functions were used as a post-processing tool in order to obtain smooth response close to $\omega_{pco}$, and were only required to match the measured response in the neighbourhood of $\omega_{pco}$ frequencies: around 4.5Hz for Configuration 1 and around 5.1Hz for Configuration 2.

$\omega_{pco}$ and $Y_f(\omega_{pco})$ are determined in two steps by inspecting Fig. 8b for Configuration 1 or Fig. 9b for Configuration 2. First, $\omega_{pco}$ is defined by the crossing of the $\Phi_f$ curve with 0deg line as indicated by the round markers in the bottom zoom-in subplots of the two figures. Next, following the vertical dashed line a crossing with the $Y_f$ curve is found which determines $Y_f(\omega_{pco})$. The corresponding crossings are marked by the round markers in the top subplots of Fig. 8b and 9b. This procedure is repeated for every measured $v_0$.

The extracted $\omega_{pco}$ and $Y_f(\omega_{pco})$ are collected in the parametric flutter margin plots (PFM plots) as a function of airstream velocity, $v_0$. $Y_f(\omega_{pco})$ gains are expressed in terms of PFM, which essentially represent the gain margin relative to 0dB. The PFM plots pertinent to Configuration 1 and 2 are shown in Figs. 10 and 11. Flutter conditions found by the conventional approach are also indicated using square markers for the sake of comparison.

Flutter conditions are then found from the PFM plots. The flutter velocity, $v_f$, is determined by finding the crossing of the PFM line with the 0dB line. The corresponding $v_f$ is indicated by the vertical dashed line in the top subplot of Fig. 10 or 11. The flutter frequency, $\omega_f$ is then found by following the dashed line until a crossing with the $\omega_{pco}$ curve in the bottom subplot of the two figures

is reached.

Summary of all the flutter results is provided in Table 2. One can observe that the agreement between all the methods, the conventional flutter test, the PFM test, and theoretical PFM method, is very good in terms of flutter speed and frequency. The observed difference in predicted flutter velocity between the conventional and the PFM test is 6% in the case of Configuration 1 and 1% in the case of Configuration 2. The agreement is even better as far as the predicted flutter frequency is concerned. In this case, the observed difference is about 0.5% for both Configuration 1 and 2. Furthermore, the differences in the case of the theoretical PFM model are of the same order of magnitude as those observed in the comparison between the conventional flutter test and the PFM test. Table 2 also provides a comparison of the measured and predicted flutter modes which are presented as heave-normalised vectors $[\zeta_{\xi f}, \zeta_{\theta f}]$, pitch-to-heave amplitude ratio, $|\zeta_{\theta f}|/|\zeta_{\xi f}|$, and the associated phase angle, $\angle(\zeta_{\theta f}/\zeta_{\xi f})$.

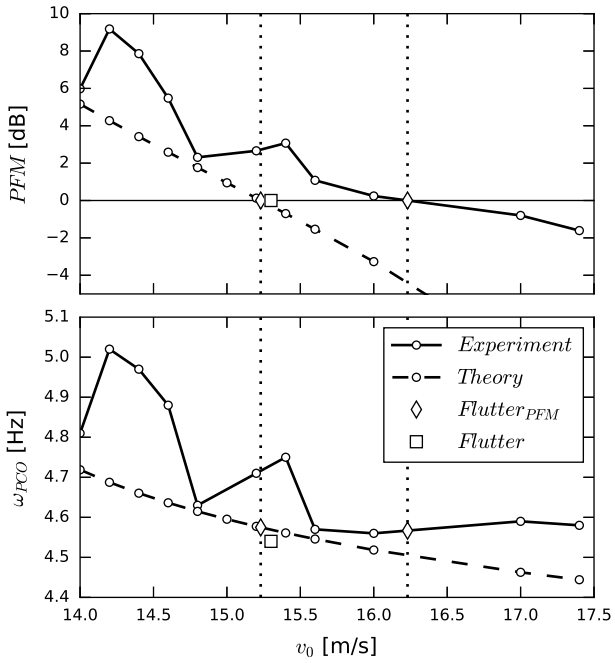


Figure 10: PFM plot: Configuration 1

By comparing the flutter modes obtained in the case of Configuration 1, one can observe some significant differences in the presented results. The flutter mode obtained by the PFM experiment contains less pitch component relative to the conventional flutter experiment, $\zeta_{\theta f}$ is reduced by 24%. In addition, the PFM experiment yields a larger phase lag of the pitch component relative to the heave component. The difference relative to the conventional flutter experiment is 35%. On the other hand, the numerical PFM method yields a

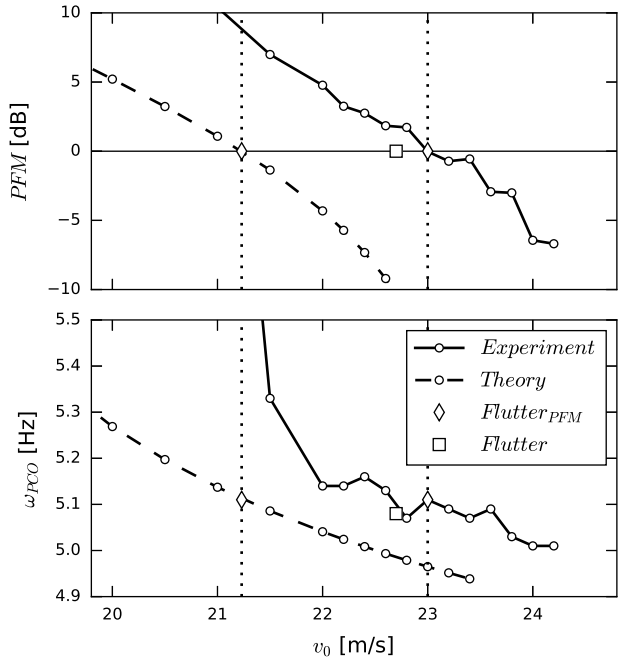


Figure 11: PFM plot: Configuration 2

flutter mode with an 11% larger pitch component in comparison to the flutter mode obtained by the conventional flutter experiment. However, the phase lag of $\zeta_{\theta f}$ is -29.3 deg which is similar to that obtained by the experimental PFM method and is 30% larger than the phase lag observed during the conventional flutter experiment.

The agreement between the different methods is very good in the case of Configuration 2. The difference in the flutter mode is about 1%, while the difference in the phase lag with respect to the conventional flutter experiment is 4% for the experimental and 2% for the numerical PFM method.

### *4.3. Divergence*

Divergence measurements using both the conventional approach and the PFM method are presented in this section. Divergence was investigated only for Configuration 1 of the aeroelastic system.

Fig. 12 shows the measurements obtained using the conventional approach, as described in Sec. 3.3.2. A typical time record of the system response in heave and pitch DOF due to small perturbation is shown in Fig. 12a. One can observe that after the transient effects die out the system remains in a new equilibrium position having increased heave and pitch displacement, $h$ and $\theta$. The difference $\Delta h$ and $\Delta\theta$ was determined from the measurements and plotted against $v_0$ as shown in Fig. 12b. Both $\Delta h$ and $\Delta\theta$ increase in magnitude with increasing $v_0$.

Table 2: Flutter results

| | Parameter | Flutter | PFM (exp.) | PFM (theory) |
|---|---|---|---|---|
| Configuration 1 | $v_f$ [m/s] | 15.3 | 16.2 (1.06)$^\dagger$ | 15.2 (0.99)$^\dagger$ |
| | $\omega_f$ [Hz] | 4.54 | 4.56 (1.004) | 4.57 (1.007) |
| | $[\zeta_{\xi f}, \zeta_{\theta f}]$ [-] | [1, 0.388 - $i$0.162] | [1, 0.276 - $i$0.162] | [1, 0.408 - $i$0.229] |
| | $\lvert\zeta_{\theta f}\rvert/\lvert\zeta_{\xi f}\rvert$ [-] | 0.420 | 0.320 (0.76) | 0.468 (1.11) |
| | $\angle(\zeta_{\theta f}/\zeta_{\xi f})$ [deg] | -22.6 | -30.4 (1.35) | -29.3 (1.30) |
| Configuration 2 | $v_f$ [m/s] | 22.7 | 23.0 (1.06) | 21.2 (0.94) |
| | $\omega_f$ [Hz] | 5.08 | 5.11 (1.004) | 5.11 (1.006) |
| | $[\zeta_{\xi f}, \zeta_{\theta f}]$ [-] | [1, 0.389 - $i$0.144] | [1, 0.394 - $i$0.139] | [1, 0.385 - $i$0.146] |
| | $\lvert\zeta_{\theta f}\rvert/\lvert\zeta_{\xi f}\rvert$ [-] | 0.415 | 0.418 (1.01) | 0.412 (0.99) |
| | $\angle(\zeta_{\theta f}/\zeta_{\xi f})$ [deg] | -20.3 | -19.4 (0.96) | -20.8 (1.02) |

$^\dagger$ relative to the results reported as Flutter.

Moreover, as the divergence speed is approached the slope of the $\Delta h$ and $\Delta\theta$ curves rapidly increases as well. Such a rapid increase, especially in the pitch DOF is observed close to 19m/s. $\Delta\theta$ increased more than three-fold due to a speed increment of 0.2m/s. $v_0 = 19$m/s is therefore considered to mark the divergence onset velocity.

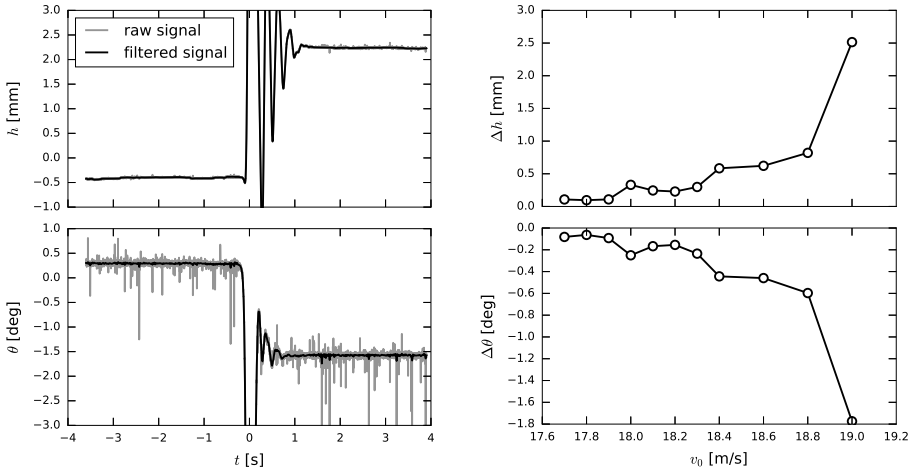


(a) Heave and pitch DOF response in time at $v_0 = 19$m/s

(b) Heave and pitch DOF discplacement as a function of velocity

Figure 12: Divergence measurement

The PFM results are presented in Fig. 13. A reference measurement used to investigate the airfoil alignment with the airstream is shown by the circular markers. The measured deflections are very small, less than 4% of those mea-

sured during the PFM experiment, indicated by the square markers, over the entire range of the investigated airstream velocities. Hence, one can conclude that the wing was well aligned with the airstream and that negligible deflections due to the initial angle of attack can be expected.

Results pertaining to the PFM experiment are represented by the square markers. Expectedly, as $v_0$ is increased both $\Delta\theta$ and $\Delta h$ increase as the wing assumes new aeroelastic equilibrium. $\Delta\theta$ reaches the value of $\theta^s$ defined by Eq. 9, indicated by the dashed horizontal line labelled $\theta^s$, at 19.4m/s, which marks the divergence onset velocity. The divergence velocity obtained with the conventional method is indicated by the dashed vertical line labeled $v_d$ for the sake of comparison. The two methods show very good agreement, with the difference of only 1%.

Numerical PFM results, depicted with diamond and triangular markers, are also shown for the sake of comparison. Results marked with diamonds were obtained using a numerical model assuming an infinite wing with a lift slope $C_{L\alpha} = 2\pi$. Results marked with triangles were obtained by correcting the $C_{L\alpha}$ coefficient for the finite span effect. The improvement is significant. The difference with respect to the experimental results is reduced from 9% to less than a 1%.

The correction is based on the $\Delta h$ measurement from the PFM experiment shown in the bottom plot of Fig. 13. In connection with the heave stiffness of the aeroelastic system the lift generated by the wing can be estimated. The results are shown in Fig. 14. The obtained results are compared to the theoretical results obtained using $C_{L\alpha} = 2\pi$ and $C_{L\alpha} = 2\pi(1 + 2/\mathit{A}\!R)$, with $\mathit{A}\!R = 2$ representing the aspect ratio of the wing. It is clear that despite mounting the end-plates on the wing, finite span effects are still present and have a significant effect on the $C_{L\alpha}$.

## 5. Conclusion

A novel method for safe experimental identification of aeroelastic instabilities based on Parametric Flutter Margins has been demonstrated by successfully predicting flutter as well as divergence onset of a 2D aeroelastic model mounted in the wind tunnel. Performing the PFM tests by adding stabilizing weight or spring, the instability points are positively identified without risking the models structural integrity.

Two different configurations of the aeroelastic model have been tested for flutter. Very good to excellent agreement between the conventional flutter test and the PFM method has been achieved. The difference in predicted flutter velocity and flutter frequency were less than 6% and less than 0.4% respectively for configuration 1. The observed differences were even smaller for configuration 2, less than 1% and less than 0.6%. Moreover, similar differences were observed in the comparison with the theoretical PFM method.

The aeroelastic system in configuration 1 was also tested for divergence. The conventional approach and the experimental PFM method show very good

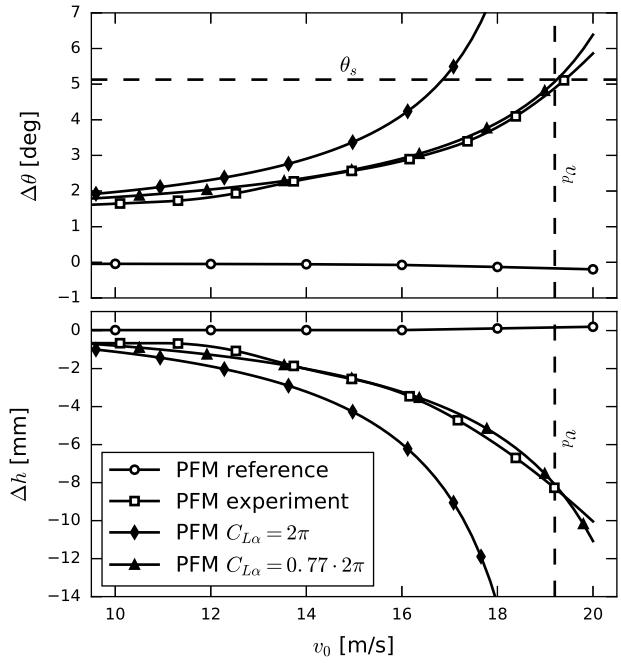


Figure 13: PFM divergence plot: Configuration 1

agreement with a difference of 1% only. The comparison between the conventional approach and the theoretical PFM method initially resulted in a moderate difference of 9% between the two methods. However, after the theoretical PFM results were corrected for the finite wing effects, the agreement was significantly improved. As a result, the observed difference was reduced to less than 1%.

A unique feature of the PFM method, that an instability boundary can be safely crossed without risking the aeroelastic model, has been demonstrated as well. This makes the performed test an important proof-of-concept milestone.

Due to its accuracy and unique properties, the PFM method marks an important contribution to the state of the art in testing for aeroelastic instabilities, with significant potential for improvement in the safety of flutter flight tests. Obviously, further wind-tunnel tests with more realistic 3D configurations and pioneering PFM-based flutter flight tests are yet to be performed for obtaining a newly established test procedure.

**Acknowledgements**

The authors would like to express their gratitude to Dr Bojan Gjerek for sharing his aeroelastic apparatus with them for conducting the aeroelastic experiments presented in this paper.

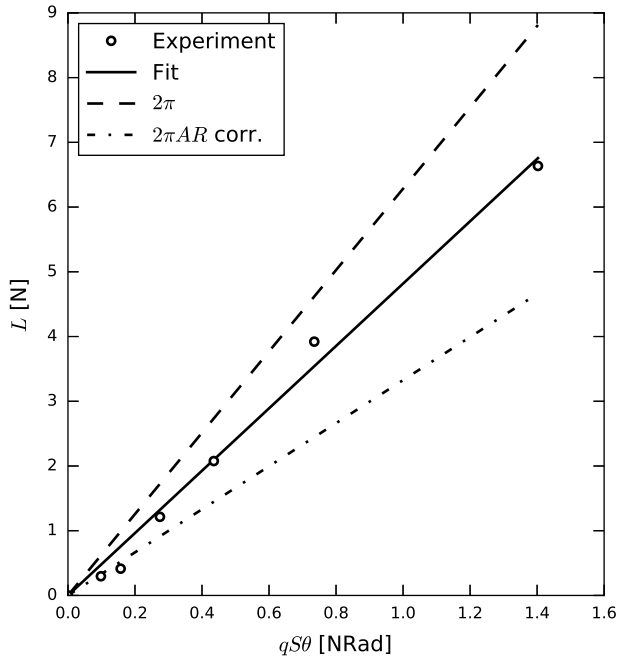


Figure 14: Finite span lift correction

The authors would also like to thank Bruce LeBlanc for his advice and help with the instrumentation of the aeroelastic system.

## References

[1] D. H. Hodges, G. A. Pierce, Introduction to structural dynamics and aeroelasticity, number 15 in Cambridge aerospace series, Cambridge University Press, New York, 2nd ed edition, 2011.

[2] M. W. Kehoe, A historical overview of flight flutter testing, NASA TM-4720 (1995).

[3] J. E. Cooper, P. R. Emmett, J. R. Wright, M. J. Schofield, Envelope function - A tool for analyzing flutter data, Journal of Aircraft 30 (1993) 785–790.

[4] J. T. Weissenburger, N. H. Zimmerman, Prediction of flutter onset speed based on flight testing at subcritical speeds, Journal of Aircraft 1 (1964) 190–202.

[5] R. Lind, M. Brenner, Flutterometer: An On-Line Tool to Predict Robust Flutter Margins, Journal of Aircraft 37 (2000) 1105–1112.

[6] H. Torii, Y. Matsuzaki, Flutter Margin Evaluation for Discrete-Time Systems, Journal of Aircraft 38 (2001) 42–47.

[7] F. Roizner, M. Karpel, Parametric Flutter Margin Method for Aeroservoelastic Stability Analysis, AIAA Journal (2017) 1–12.

[8] M. Karpel, F. Roizner, Towards Flutter-Boundary Tests with Controlled Vibration Levels, in: Proceedings of the Israel Annual Conference on Aerospace Sciences (IACAS), Tel Aviv, Israel.

[9] T. Theodorsen, General theory of aerodynamic instability and the mechanism of flutter, NACA REPORT No. 496 (1935) 413–433.

[10] H. J. Hassig, An Approximate True Damping Solution of the Flutter Equation by Determinant Iteration, Journal of Aircraft 8 (1971) 885–889.

[11] P. C. Chen, Damping Perturbation Method for Flutter Solution: The g-Method, AIAA Journal 38 (2000).

[12] B. Gjerek, R. Drazumeric, F. Kosel, A Novel Experimental Setup for Multiparameter Aeroelastic Wind Tunnel Tests, Experimental Techniques 38 (2014) 30–43.